JACS
JOURNAL OF THE AMERICAN CHEMICAL SOCIETY

pubs.acs.org/JACS

Communication

Mixed-Metal Alloying in Hybrid Bronzes

Anton F. Walte, Raúl Torres-Cadena, W. Lakna N. Dayaratne, and Adam Jaffe*

Cite This: J. Am. Chem. Soc. 2024, 146, 23699−23703

Read Online

ACCESS | Metrics & More | Article Recommendations | Supporting Information

ABSTRACT: We show that substitutional alloying during the aqueous self-assembly of layered organic-templated metal oxides produces single-phase mixed-metal hybrids. Single-crystal X-ray diffraction, bulk elemental analyses, and vibrational and electronic spectroscopies corroborate a solid solution of Mo and W atoms at lattice sites within the two-dimensional metal oxide layers. Mild postsynthetic reduction then introduces relatively delocalized electrons to afford mixed-metal hybrid bronzes. To our knowledge, this represents the first demonstration of mixed-metal alloying in a hybrid metal oxide and a rare example of solid-solution formation at low temperature. We show this approach yields mixed-metal congeners with optical band gaps over 130 meV smaller than those of single-metal analogs, while achieving activation energies (E_a) of conduction as low as 78.4(2) meV. Further, metal substitution appears to tune collective electronic phenomena by suppressing the non-Arrhenius behavior observed for Mo-based hybrids. This work considerably expands the nascent hybrid bronze platform to help address energy-related challenges and fundamental solid-state physical questions.

We recently described *hybrid bronzes* as mixed-valence organic−inorganic materials featuring alternating two-dimensional layers of (a) metal oxides with tunable electronic structures that support appreciable concentrations of charge carriers and (b) arrays of organic species that introduce molecular functionality and structure-directing behavior.[1] Hybrid bronzes are air- and water-stable and are readily synthesized under mild aqueous conditions, in contrast to many of their inorganic metal-oxide bronze parent materials of the form A_xMO_y (A = cation; M = Mo, W, V; *x*, *y* depend on metal valence) that are formed at high temperature and/or are difficult to tune synthetically.[2] The inorganic compounds' moniker "bronze" originates from their reflectivity resulting from a high concentration of quasi-free electrons. The combination of these mobile charge carriers along with tunable electronic structures in inorganic metal-oxide bronzes has motivated their decades-long study related to energy-storage,[3] optoelectronics,[4] catalysis,[5] and solid-state physical phenomena such as superconductivity,[6] spin-glass behavior,[7] and charge-density wave states.[8] By integrating mixed-valence 2D metal oxide layers with ordered arrays of potentially redox-, photo-, or chemically active small molecules, hybrid bronzes place (opto)electronically active and conductive metal-oxide bronze sheets in proximity to molecular species that provide greater chemical diversity and tunability but which would not otherwise normally support long-range charge transport.

In our previous work, after drawing inspiration from reported hybrid oxides,[9] we developed the hybrid bronze platform by targeting: (a) synthetic reduction level control[1a] and (b) molecular templation to control the inorganic connectivity, thereby modulating electronic structure.[1b] Another untapped strategy for control of electronic properties such as band gap, conductivity, and redox activity is compositional alloying—i.e., atomic substitution at lattice sites—a method exercised to great effect for inorganic metal oxides,[10] recently in halide perovskites,[11] and naturally in bronze, the namesake copper−tin alloy itself. In this work, we demonstrate alloyed mixed-metal hybrid bronzes based on molybdenum and tungsten (Figure 1) by employing single-crystal and powder X-ray diffraction, Raman spectroscopy, and bulk elemental analyses. Diffuse reflectance spectroscopy and charge transport measurements show that this substitution—which alters the orbital composition of the materials' electronic bands—leads to observable changes in the optical and electronic behavior of mixed-metal systems relative to their single-metal congeners. We therefore demonstrate this approach's potential for tuning key (opto)electronic properties of hybrid bronzes, such as light absorption and charge transport.

Combining $(NH_4)_6Mo_7O_{24}{\cdot}4H_2O$ and $(NH_4)_6H_2W_{12}O_{40}{\cdot}xH_2O$ in a nominal equimolar Mo:W ratio, together with 4,4′-bipyridine (4,4′-bipy), pyrazine (pyz), or 4*H*-1,2,4-triazole (4*H*-trz) under hydrothermal conditions ca. 150−170 °C for 3 days, afforded crystals suitable for X-ray structure determination of $(4,4'\text{-bipy})_{0.5}Mo_{0.20}W_{0.80}O_3$, $(pyz)_{0.5}H_{0.1}Mo_{0.24}W_{0.76}O_3$, and $(4H\text{-trz})_{0.5}Mo_{0.63}W_{0.37}O_3$, respectively (Figure 1). Single-metal structural models featuring solely molybdenum or tungsten centers did not account for the observed electron density at the metal sites, producing nonphysical/improbable site occupancies such as 1.75 for Mo or 0.88 for W in the 4,4′-bipy-templated case (see Supporting Information for discussion). Instead, models featuring fully occupied metal sites with a freely refined

Received: July 3, 2024
Revised: August 9, 2024
Accepted: August 12, 2024
Published: August 19, 2024

https://doi.org/10.1021/jacs.4c08960
J. Am. Chem. Soc. 2024, 146, 23699−23703

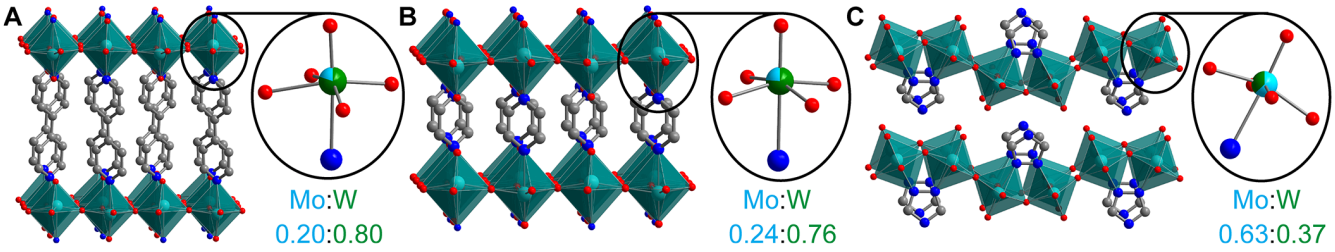

Figure 1. X-ray structures of (A) $(4,4'\text{-bipy})_{0.5}Mo_{0.20}W_{0.80}O_3$, (B) $(pyz)_{0.5}H_{0.1}Mo_{0.24}W_{0.76}O_3$, and (C) $(4H\text{-trz})_{0.5}Mo_{0.63}W_{0.37}O_3$. Gray, blue, red, and teal spheres are C, N, O, and mixed W/Mo sites, respectively. Polyhedra illustrate connectivity. H atoms and disorder are omitted for clarity. Insets: isolated metal sites showing Mo:W ratios via light blue and green sectors, respectively.

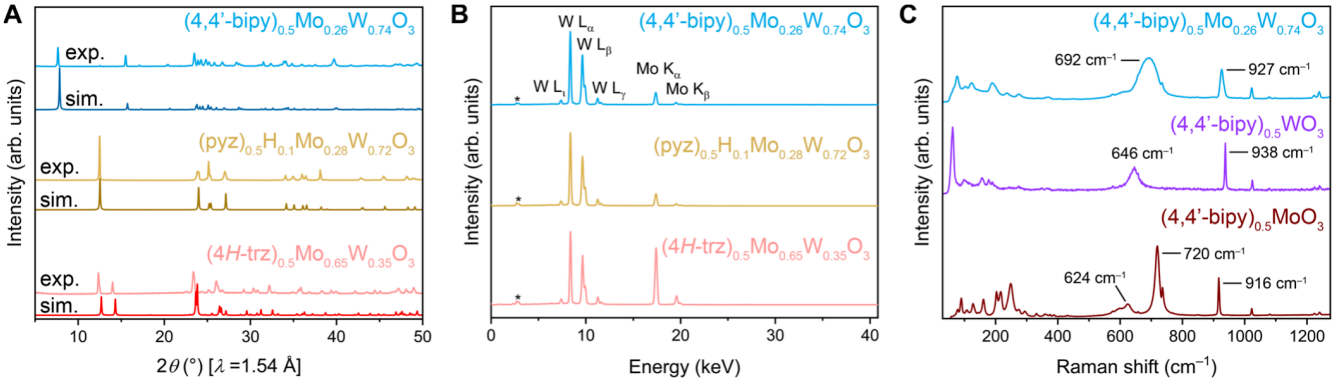

Figure 2. (A) Powder X-ray diffraction patterns of mixed-metal hybrid oxides templated by 4,4′-bipy, pyz, and 4*H*-trz. Patterns simulated from single-crystal structures are shown for reference. (B) X-ray fluorescence spectra showing the presence of both Mo and W. Asterisks indicate background peaks. (C) Raman spectrum of $(4,4'\text{-bipy})_{0.5}Mo_{0.26}W_{0.74}O_3$ shown in comparison to the single-metal W and Mo analogs.[1a]

Mo:W ratio and no evidence of preferential ordering—a solid solution—yielded excellent fits to the data. Intriguingly, while the 4,4′-bipy- and pyz-templated structures gave Mo:W ratios of approximately 1:4 and 1:3, respectively, the 4*H*-trz-templated analog yielded a higher Mo content with a ratio closer to 2:1. This divergent behavior alludes to the importance of molecular templation effects in dictating the final structure, including metal content. We note that the pyz-templated material formed black crystals that, when coupled with the electronic and optical characterization described below, indicates the reaction conditions were sufficiently reducing to produce the mixed-valence hybrid bronze instead of the oxidized form. Hence, we include charge-balancing protons in the formula above, though oxygen vacancies are also possible.

To confirm bulk homogeneity, we measured powder X-ray diffraction (PXRD) patterns of ground material from hydrothermal syntheses. These room-temperature data match simulated patterns from our single-crystal X-ray structures collected at 120 K, aside from peak shifts attributable to differing measurement temperatures (Figure 2A). Inductively coupled plasma−optical emission spectrometry (ICP-OES) analysis yielded Mo:W ratios of 26:74, 28:72, and 65:35 for the 4,4′-bipy-, pyz-, and 4*H*-trz-templated materials (Table S1), respectively, in agreement with the single-crystal X-ray structures. X-ray fluorescence analysis (Figures 2B, S1; Table S1) confirms similar values. Unless otherwise stated, we use Mo:W ratios determined by ICP-OES in compound formulas, owing to this method's accuracy. Importantly, using $(4,4'\text{-bipy})_{0.5}Mo_{0.42}W_{0.58}O_3$ as a representative example, we were also able to isolate microcrystalline material without the use of cumbersome hydrothermal pressure vessels through the rapid and mild method we previously reported that only requires stirring precursors in water for 24 h at 80 °C (Figures S2–S3).[1a]

We collected Raman spectra on powder samples to probe how alloying perturbs metal−oxygen vibrational modes (Figures 2C, S4–S5).[1a] Considering the 4,4′-bipy-templated case as an example (Figure 2C), features between 600−750 cm^{-1} are attributable to bridging (μ_2) oxo modes while those ca. 900−950 cm^{-1} are assigned to terminal (μ_1) M=O oxos. We note that modes between 600−750 cm^{-1} are split in the Mo-only case but not for W analogs. This divergent bonding behavior is corroborated by M−μ_2-O bond distance analysis (Table S2): MoO_5N octahedra are distorted, featuring two shorter and two longer M−μ_2-O bonds while WO_5N octahedra are more regular (more similar bridging metal−oxygen bond lengths). In the spectrum of $(4,4'\text{-bipy})_{0.5}Mo_{0.26}W_{0.74}O_3$, the μ_2-oxo mode at 692 cm^{-1} and the μ_1-oxo mode at 927 cm^{-1} are at intermediate values between those observed for the single-metal hybrids and they show no splitting, implying both a single-phase and more regular octahedra.

We acquired UV−visible diffuse reflectance spectra to explore the (opto)electronic effects of mixed-metal substitution in hybrid oxides (Figure 3). In comparison to the single-metal materials, the mixed-metal hybrids $(4,4'\text{-bipy})_{0.5}Mo_{0.14}W_{0.86}O_3$ and $(4H\text{-trz})_{0.5}Mo_{0.66}W_{0.34}O_3$ display absorption edges red-shifted by ca. 130 meV (Figures S6–S7). These edges are assigned to transitions from nonbonding O 2p-derived valence bands to antibonding metal d-derived conduction bands.[9g,12] Since the pyz-templated hybrid is reduced during synthesis, we did not acquire a spectrum for its oxidized form. However, an absorption peak centered at ca.

https://doi.org/10.1021/jacs.4c08960
J. Am. Chem. Soc. 2024, 146, 23699−23703

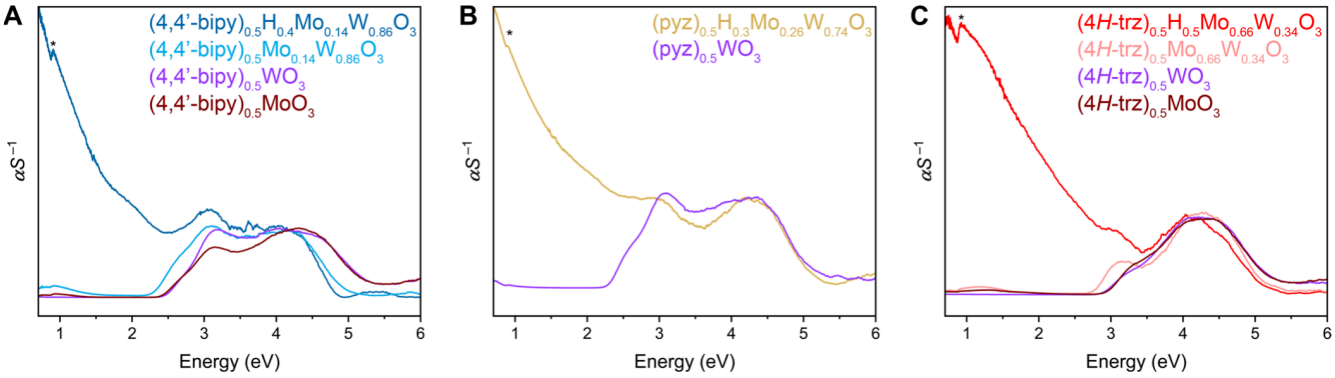

Figure 3. Diffuse reflectance spectra for mixed-metal hybrid oxides and their hybrid bronzes, templated by (A) 4,4′-bipy, (B) pyz, and (C) 4*H*-trz, respectively, and shown in comparison to single-metal congeners. Spectra are normalized to the high-energy feature ca. 4.5 eV. Asterisks denote $BaSO_4$ background peaks.

2.97 eV is observed in $(pyz)_{0.5}H_{0.3}Mo_{0.26}W_{0.74}O_3$—approximately 130 meV lower than the analogous feature in $(pyz)_{0.5}WO_3$. Overall, these data suggest that mixed-metal alloying appreciably diminishes the optical band gap within this family of hybrid metal oxides. Similar band gap narrowing has been observed in inorganic mixed Mo/W oxide hydrates.[13]

To understand the anomalously diminished mixed-metal material band gaps (Table S3), we consider the unexpectedly similar single-metal analogs' gaps defined by their conduction band minimum (CBM) and valence band maximum (VBM)—dictated both by band position (in energy) and dispersion. Though it is challenging to deconvolute contributing factors, they may include: (1) Mo 4d states are lower-energy than W 5d,[14] comparatively lowering the Mo conduction band position and CBM. In parallel, (2) molybdenum is more electronegative,[15] lowering this materials' VBM by stabilizing oxygen orbitals comprising the valence band. Additionally, (3) metal−oxygen lattice distortion may alter oxygen orbital overlap for the Bloch waves defining the valence band dispersion, raising/lowering the VBM depending on distortion type. Multiple interplaying effects can thus yield similar single-metal band gaps. Now, in mixed-metal materials, lower-energy Mo 4d states in the conduction band should stabilize the CBM relative to W-only materials, while lower average metal electronegativity should elevate O 2p states at the VBM, raising it relative to Mo-only materials. Intermediate lattice distortion compared to single-metal cases may also yield intermediate valence band dispersion and further adjust the VBM. Ultimately, alloying can therefore yield smaller band gaps than single-metal materials (additional discussion in Supporting Information). Future electronic structure studies will continue elucidating this behavior.

To produce hybrid bronzes from the alloyed Mo−W hybrid oxides, we controlled their mixed-valency through mild postsynthetic reduction with sodium dithionite. X-ray photoelectron spectroscopy (XPS) analysis (Figures S8−S11) indicates preferential Mo reduction, likely attributable to the higher $Mo^{6+/5+}$ reduction potential (0.36 V vs SHE[1a]) compared to $W^{6+/5+}$ (0.13 V vs SHE[16]). We assign the resulting hybrid bronze formulas as $(L)_{0.5}H_xMO_3$ (M = mixed-Mo/W site) with x = 0.4, 0.3, and 0.5 for L = 4,4′-bipy, pyz, and 4*H*-trz, respectively, since proton insertion is the likely mechanism of charge-balance (see Supporting Information). This mechanism and proton behavior within hybrid bronzes will be explored in future work.

Diffuse reflectance spectra corroborate reduction of mixed-metal samples and the corresponding introduction of more mobile electrons. New, strong absorption features whose intensities increase with decreasing energy are observed across the visible and near-infrared spectrum from ca. 3−0.7 eV (Figure 3). This behavior is attributable to charge carrier population of the conduction band. Like the single-metal cases,[1] no peak is observed that would indicate either plasmonic resonance,[17] strongly localized intervalence charge transfer (IVCT),[18] or strongly localized polarons.[19] For IVCT,[18] Hush predicted a peak at four times the activation barrier energy (E_a') for symmetrical one-electron transfer. Strongly localized polarons—charge carriers self-localized through electron−lattice coupling—would also require optical excitation in the visible or near-infrared to surmount a relatively large E_a' for hopping to neighboring undistorted sites. The absence of a peak is consistent with less strongly localized IVCT/polaronic hopping processes with small E_a'.

We turned to variable temperature conductivity (σ) measurements to understand the effect of mixed-metal alloying on charge transport (Figures 4, S12). These data are well-modeled by either Arrhenius-type $\ln(\sigma)$ vs $1/T$ linear fits or polaronic-type $\ln(\sigma T)$ vs $1/T$ linear fits. Thus, discerning contributions from lattice vibration coupling is challenging. This mixed-metal behavior is similar to the linear Arrhenius/polaronic trends we previously observed for the tungsten-based hybrid bronzes, in contrast to significant nonlinearity for the molybdenum-based materials that may indicate charge-density wave-like contributions.[1a,20] Increased regularity of the M−O bonds in mixed-metal hybrids, higher W content and more dispersed bands, and/or metal-site disorder may explain this behavior. Linear fits to the Arrhenius model yield low E_a values of 78.4(2) and 93.7(3) meV for the 4,4′-bipy- and pyz-based mixed-metal materials, respectively, indicating facile transport. These values are similar to $(4,4'\text{-bipy})_{0.5}H_{0.7}WO_3$ (52(3) meV), $(4,4'\text{-bipy})_{0.5}H_{0.47}MoO_3$ (ca. 139 meV), and $(pyz)_{0.5}H_{0.44}MoO_3$ (ca. 92 meV) from our prior work.[1a] The mixed-metal congeners exhibit lower room-temperature conductivity values (ca. 10^{-6}−10^{-5} S/cm, Table S4) than the single-metal analogs (ca. 10^{-5}−10^{-2} S/cm). This may result from lower carrier mobility, e.g., from scattering induced by metal-site disorder, or from lower effective carrier concentration if some electrons introduced during reduction remain localized. We note that grain boundary resistance likely leads to underestimated conductivities.

https://doi.org/10.1021/jacs.4c08960
J. Am. Chem. Soc. 2024, 146, 23699−23703

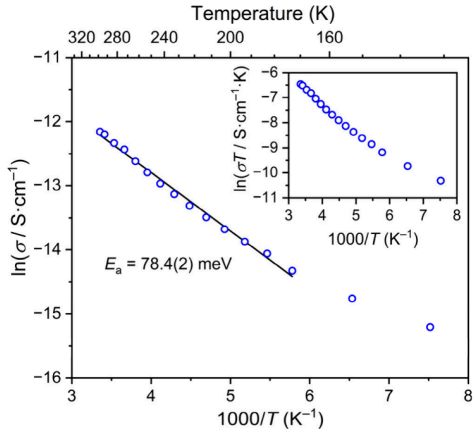

Figure 4. Variable-temperature four-point conductivity measurements on a pellet of $(4,4'\text{-bipy})_{0.5}H_{0.4}Mo_{0.14}W_{0.86}O_3$ plotted as $\ln(\sigma)$ vs $1000/T$ (linearized Arrhenius equation) with a fitted activation energy above 173 K. Inset: data according to the polaronic model.

Herein, we have shown that the (opto)electronic behavior of mixed-valence organic−inorganic metal oxides called hybrid bronzes can be tuned through mild mixed-metal alloying to yield solid solutions of Mo and W at metal lattice sites with no evidence of ordering. To our knowledge, this is the first demonstration of mixed-metal alloying in hybrid oxides and a rare example of solid solution formation under mild conditions. Postsynthetic chemical reduction produces mixed-metal hybrid bronzes by introducing quasi-delocalized charge carriers. In our approach, we have demonstrated reduction of the hybrids' band gaps by ca. 130 meV and alteration of their variable-temperature conductivity behavior that connotes modulation of collective electronic phenomena, while maintaining facile transport (low hopping barriers). Mixed-metal alloying therefore holds promise for simultaneous control of electronic structure and charge transport in hybrid bronzes, thereby expanding the potential reach of the hybrid bronze platform for addressing crucial energy-related challenges and demonstrating important solid-state phenomena.

■ ASSOCIATED CONTENT

Supporting Information

The Supporting Information is available free of charge at https://pubs.acs.org/doi/10.1021/jacs.4c08960.

Experimental details, diffraction patterns, spectra, elemental analysis, and supplemental discussion (PDF)

Accession Codes

CCDC 2352096−2352098 contain the supplementary crystallographic data for this paper. These data can be obtained free of charge via www.ccdc.cam.ac.uk/data_request/cif, or by emailing data_request@ccdc.cam.ac.uk, or by contacting The Cambridge Crystallographic Data Centre, 12 Union Road, Cambridge CB2 1EZ, UK; fax: +44 1223 336033.

■ AUTHOR INFORMATION

Corresponding Author

Adam Jaffe − *Department of Chemistry and Biochemistry, University of Notre Dame, Notre Dame, Indiana 46556, United States;* orcid.org/0000-0002-9886-0249; Email: ajaffe@nd.edu

Authors

Anton F. Walte − *Department of Chemistry and Biochemistry, University of Notre Dame, Notre Dame, Indiana 46556, United States;* orcid.org/0009-0000-8602-0093

Raúl Torres-Cadena − *Department of Chemistry and Biochemistry, University of Notre Dame, Notre Dame, Indiana 46556, United States;* orcid.org/0000-0001-8832-7806

W. Lakna N. Dayaratne − *Department of Chemistry and Biochemistry, University of Notre Dame, Notre Dame, Indiana 46556, United States;* orcid.org/0000-0001-5051-1835

Complete contact information is available at: https://pubs.acs.org/10.1021/jacs.4c08960

Notes

The authors declare no competing financial interest.

■ ACKNOWLEDGMENTS

This material is based upon work supported by the National Science Foundation under Award No. DMR-2338086. X-ray diffraction studies were carried out at the Notre Dame Molecular Structure Facility. We thank the ND Energy Materials Characterization Facility (MCF) for the use of the UV−visible spectrometer, the X-ray fluorescence spectrometer, and X-ray photoelectron spectrometer which were utilized to acquire diffuse reflectance, XRF, and XPS measurements, respectively. The MCF is funded by the Sustainable Energy Initiative (SEI), which is part of the Center for Sustainable Energy at Notre Dame (ND Energy). Additional XPS spectra were collected at the College of Science and Engineering Characterization Facility at the University of Minnesota. We acquired variable temperature conductivity measurements at the Analytical Science and Engineering at Notre Dame (ASEND) Core Facility. We collected ICP-OES measurements at the Center for Environmental Science and Technology (CEST). We thank Dr. Allen Oliver for assistance with X-ray diffraction studies, Dr. Ian Lightcap and Anna Matzner for assistance with XPS, and Jon Loftus for his assistance with ICP-OES measurements.

■ REFERENCES

(1) (a) Dayaratne, W. L. N.; Torres-Cadena, R.; Schmitt, B. P.; Westrick, E. M.; Jaffe, A. Hybrid bronzes: mixed-valence organic-inorganic metal oxides as a tunable material platform. *Chem. Sci.* **2023**, *14*, 10756−10767. (b) Wan, S.; Musielak, N.; Oliver, A. G.; Jaffe, A. Controlling Electron Delocalization in Vanadium-Based Hybrid Bronzes through Molecular Templation. *Angew. Chem., Int. Ed.* **2023**, *62*, e202314523.

(2) (a) Dickens, P. G.; Whittingham, M. S. The tungsten bronzes and related compounds. *Q. Rev., Chem. Soc.* **1968**, *22*, 30−44. (b) Greenblatt, M. Molybdenum oxide bronzes with quasi-low-dimensional properties. *Chem. Rev.* **1988**, *88*, 31−53. (c) Marley, P. M.; Horrocks, G. A.; Pelcher, K. E.; Banerjee, S. Transformers: the changing phases of low-dimensional vanadium oxide bronzes. *Chem. Commun.* **2015**, *51*, 5181−5198.

(3) Chernova, N. A.; Roppolo, M.; Dillon, A. C.; Whittingham, M. S. Layered vanadium and molybdenum oxides: batteries and electrochromics. *J. Mater. Chem.* **2009**, *19*, 2526−2552.

(4) Yu, X.; Marks, T. J.; Facchetti, A. Metal oxides for optoelectronic applications. *Nat. Mater.* **2016**, *15*, 383−396.

(5) Zhang, Z.; Liu, J.; Gu, J.; Su, L.; Cheng, L. An overview on metal oxide materials as electrocatalysts and supports for polymer electrolyte fuel cells. *Energy Environ. Sci.* **2014**, *7*, 2535−2558.

(6) Raub, C. J.; Sweedler, A. R.; Jensen, M. A.; Broadston, S.; Matthias, B. T. Superconductivity of Sodium Tungsten Bronzes. *Phys. Rev. Lett.* **1964**, *13*, 746−747.
(7) Sotani, N.; Fukumoto, T.; Eda, K.; Kunitomo, M.; Nakagawa, M. Spin-Glass Behavior of Hydrogen Molybdenum Bronze, H_xMoO_3. *Chem. Lett.* **1999**, *28*, 593−594.
(8) Rousseau, R.; Canadell, E.; Alemany, P.; Galván, D.; Hoffmann, R. Origin of the Metal-to-Insulator Transition in $H_{0.33}MoO_3$. *Inorg. Chem.* **1997**, *36*, 4627−4632.
(9) (a) Johnson, J. W.; Jacobson, A. J.; Rich, S. M.; Brody, J. F. New layered compounds with transition-metal oxide layers separated by covalently bound organic ligands. Molybdenum and tungsten trioxide-pyridine. *J. Am. Chem. Soc.* **1981**, *103*, 5246−5247. (b) Zhang, Y.; Haushalter, R. C.; Clearfield, A. Hydrothermal Syntheses and Structural Characterization of Layered Vanadium Oxides Incorporating Organic Cations: α-, β-$(H_3N(CH_2)_2NH_3)[V_4O_{10}]$ and α-, β-$(H_2N(C_2H_4)_2NH_2)[V_4O_{10}]$. *Inorg. Chem.* **1996**, *35*, 4950−4956. (c) Hagrman, P. J.; Hagrman, D.; Zubieta, J. Organic−Inorganic Hybrid Materials: From "Simple" Coordination Polymers to Organodiamine-Templated Molybdenum Oxides. *Angew. Chem., Int. Ed.* **1999**, *38*, 2638−2684. (d) Yan, B.; Xu, Y.; Goh, N. K.; Chia, L. S. Hydrothermal synthesis and crystal structures of two novel hybrid open-frameworks and a two-dimensional network based on tungsten(VI) oxides. *Chem. Commun.* **2000**, 2169−2170. (e) Yan, B.; Luo, J.; Dube, P.; Sefat, A. S.; Greedan, J. E.; Maggard, P. A. Spin-Gap Formation and Thermal Structural Studies in Reduced Hybrid Layered Vanadates. *Inorg. Chem.* **2006**, *45*, 5109−5118. (f) Islah-u-din; Fox, M. R.; Martin, H.; Gainsford, G. J.; Kennedy, J.; Markwitz, A.; Telfer, S. G.; Jameson, G. B.; Tallon, J. L. Synthesis and structure of Na^+-intercalated WO_3(4,4'-bipyridyl)$_{0.5}$. *Chem. Commun.* **2010**, *46*, 4261−4263. (g) Zhang, X.; Hejazi, M.; Thiagarajan, S. J.; Woerner, W. R.; Banerjee, D.; Emge, T. J.; Xu, W.; Teat, S. J.; Gong, Q.; Safari, A.; Yang, R.; Parise, J. B.; Li, J. From 1D Chain to 3D Network: A New Family of Inorganic−Organic Hybrid Semiconductors $MO_3(L)_x$ (M = Mo, W; L = Organic Linker) Built on Perovskite-like Structure Modules. *J. Am. Chem. Soc.* **2013**, *135*, 17401−17407. (h) Fernández de Luis, R.; Orive, J.; Larrea, E. S.; Karmele Urtiaga, M.; Arriortua, M. I. Hybrid vanadates constructed from extended metal−organic arrays: crystal architectures and properties. *CrystEngComm* **2014**, *16*, 10332−10366.
(10) West, A. R. *Solid state chemistry and its applications*, 2nd ed.; John Wiley & Sons, Inc.: Chichester, West Sussex, U.K., 2014.
(11) (a) Lindquist, K. P.; Mack, S. A.; Slavney, A. H.; Leppert, L.; Gold-Parker, A.; Stebbins, J. F.; Salleo, A.; Toney, M. F.; Neaton, J. B.; Karunadasa, H. I. Tuning the bandgap of $Cs_2AgBiBr_6$ through dilute tin alloying. *Chem. Sci.* **2019**, *10*, 10620−10628. (b) Wolf, N. R.; Connor, B. A.; Slavney, A. H.; Karunadasa, H. I. Doubling the Stakes: The Promise of Halide Double Perovskites. *Angew. Chem., Int. Ed.* **2021**, *60*, 16264−16278.
(12) (a) Canadell, E.; Whangbo, M.-H. Conceptual aspects of structure-property correlations and electronic instabilities, with applications to low-dimensional transition-metal oxides. *Chem. Rev.* **1991**, *91*, 965−1034. (b) Sekikawa, T.; Tallon, J. L.; Chong, S. V.; Ōno, Y. Electronic Structure of a Layered Organic−Inorganic Hybrid Material $(WO_3)_2$(4,4′-bipyridyl) Based on the First-principles Calculation. *J. Phys. Soc. Jpn.* **2023**, *92*, 023702.
(13) Zhou, L.; Zhu, J.; Yu, M.; Huang, X.; Li, Z.; Wang, Y.; Yu, C. $Mo_xW_{1-x}O_3$·0. $33H_2O$ Solid Solutions with Tunable Band Gaps. *J. Phys. Chem. C* **2010**, *114*, 20947−20954.
(14) Mann, J. B.; Meek, T. L.; Knight, E. T.; Capitani, J. F.; Allen, L. C. Configuration Energies of the d-Block Elements. *J. Am. Chem. Soc.* **2000**, *122*, 5132−5137.
(15) Sanderson, R. T. Electronegativity and bonding of transitional elements. *Inorg. Chem.* **1986**, *25*, 3518−3522.
(16) Zhen, Y.; Jelle, B. P.; Gao, T. Electrochromic properties of WO_3 thin films: The role of film thickness. *Anal. Sci. Adv.* **2020**, *1*, 124−131.
(17) (a) Cheng, H.; Wen, M.; Ma, X.; Kuwahara, Y.; Mori, K.; Dai, Y.; Huang, B.; Yamashita, H. Hydrogen Doped Metal Oxide Semiconductors with Exceptional and Tunable Localized Surface Plasmon Resonances. *J. Am. Chem. Soc.* **2016**, *138*, 9316−9324. (b) Kuwahara, Y.; Yoshimura, Y.; Haematsu, K.; Yamashita, H. Mild Deoxygenation of Sulfoxides over Plasmonic Molybdenum Oxide Hybrid with Dramatic Activity Enhancement under Visible Light. *J. Am. Chem. Soc.* **2018**, *140*, 9203−9210.
(18) (a) Hush, N. S. Homogeneous and heterogeneous optical and thermal electron transfer. *Electrochim. Acta* **1968**, *13*, 1005−1023. (b) Hush, N. S. Distance Dependence of Electron Transfer Rates. *Coord. Chem. Rev.* **1985**, *64*, 135−157.
(19) (a) Schirmer, O. F.; Salje, E. The W^{5+} polaron in crystalline low temperature WO_3 ESR and optical absorption. *Solid State Commun.* **1980**, *33*, 333−336. (b) Emin, D. Optical properties of large and small polarons and bipolarons. *Phys. Rev. B: Condens. Matter Mater. Phys.* **1993**, *48*, 13691−13702. (c) Schirmer, O. F.; Wittwer, V.; Baur, G.; Brandt, G. Dependence of WO_3 Electrochromic Absorption on Crystallinity. *J. Electrochem. Soc.* **1977**, *124*, 749−753. (d) He, T.; Yao, J. Photochromism of molybdenum oxide. *J. Photochem. Photobiol., C* **2003**, *4*, 125−143. (e) Raj, S.; Sato, T.; Souma, S.; Takahashi, T.; Sarma, D. D.; Mahadevan, P. Metal-Insulator Transition of Na_xWO_3 Studied by Angle-Resolved Photoemission Spectroscopy. *Mod. Phys. Lett. B* **2009**, *23*, 2819−2846.
(20) Adams, S. CDW Superstructures in Hydrogen Molybdenum Bronzes H_xMoO_3. *J. Solid State Chem.* **2000**, *149*, 75−87.

https://doi.org/10.1021/jacs.4c08960
J. Am. Chem. Soc. 2024, 146, 23699−23703